

## Photocatalytic decolorization of indigo-carmin dye by sol-gel synthesized doped ZrO<sub>2</sub> photocatalyst

Belkacem Ziane<sup>1,2,\*</sup>, Messaoud Chaib<sup>1</sup>, Mohamed Badaoui<sup>1,2</sup>

<sup>1</sup>Département de chimie, Faculty of Sciences of the Matter, Ibn Khaldoun University of Tiaret, BP 78 Zaaroura, Tiaret, Algeria

<sup>2</sup>Département de Chimie, Faculty of Sciences, Djilali-liabes University, BP 89 City Elarbi-Ben m'hidi Sidi Belabbes, Algeria

\*corresponding author e-mail address: [zbelkacem@gmail.com](mailto:zbelkacem@gmail.com)

### ABSTRACT

The effect of transition metal dopants (Mn<sup>2+</sup>, Fe<sup>2+</sup>, Co<sup>2+</sup>, Ni<sup>2+</sup>, and Cu<sup>2+</sup>) on the photocatalytic properties of ZrO<sub>2</sub> was investigated. Crystallized powders of photocatalyst synthesized by Sol-gel process with zirconium n-butoxide and tert-butyl alcohol precursors were characterized by X-ray diffraction, UV-Vis diffuse reflectance, nitrogen adsorption isotherms and energy dispersive X-ray (EDX) analysis. Photocatalytic activity under UV irradiation of undoped and doped ZrO<sub>2</sub> powders was tested by degradation of indigo carmine dye, chosen as model the organic pollutant. Doping of ZrO<sub>2</sub> with Nickel, Cobalt, Manganese and Copper decreases the Crystallite size of powders except of Iron. Comparison of photocatalytic activity of undoped and doped ZrO<sub>2</sub> photocatalyst shows that doping with Manganese and Iron increases the efficiency of degradation of studied pollutant.

**Keywords:** Photocatalysis; ZrO<sub>2</sub>; Transition metals; Sol-gel; Indigo carmine.

### 1. INTRODUCTION

Removal of toxic pollutants from wastewater is a real challenge for scientists. Dyes are an important class of aquatic pollutants and are becoming a major source of environmental contamination [1]. Indigo carmine dye is used in food industry, cosmetics industries and also for dyeing of denim and polyester fibers. Indigo carmine is a highly toxic which might cause irritations vomiting and diarrhoea to human beings [2, 3]. Several methods like adsorption, osmosis, flocculation and others have been used for dye removal from water [4]. Photocatalysis is one of the most promising techniques that can be used efficiently to achieve high removal rates of pollutants [5]. Photocatalysis is a process based on absorption of energy (visible or UV light) by a bulky semiconductor [6].

The degradation reactions take place in the interphase region between the liquid and photo excited solid. Heterogeneously dispersed semiconductor surfaces provide a fixed environment to influence the chemical reactivity of a wide range of adsorbates and a means to initiate light-induced redox reactivity in these weakly associated molecules [7]. This technology can

provide advantages over other process, but it is limited to low concentrations of pollutants [8]. Among various transition metal oxides, zirconium oxide (zirconia, ZrO<sub>2</sub>) has been considered as an important material due to several unique properties that make it versatile for a number of applications [9]. It was used as a photocatalyst in photochemical heterogeneous reactions [10]. ZrO<sub>2</sub> possesses properties such as thermal stability, high specific surface area, and other optical and electrical properties that make it an attractive photocatalyst [11, 12].

The incorporation of dopants into the zirconia structure modifies its properties allowing the control of its microstructure [13]. Recently, it has been demonstrated that pure ZrO<sub>2</sub> waveguides can be elaborated by the sol-gel method [14, 15].

The present study involves the photocatalytic degradation of indigo-carmin dye by heterogeneous photocatalytic process using pure and transition metals doped ZrO<sub>2</sub> prepared by a sol-gel technique and characterized by X ray diffraction, UV/Vis spectroscopy, BET, and SEM/EDX techniques.

### 2. EXPERIMENTAL SECTION

#### 2.1. Materials and methods.

##### 2.1.1. Samples preparation.

The typical synthesis procedure of ZrO<sub>2</sub> and metal doped-ZrO<sub>2</sub> is as follows: 6mL of deionized water was mixed with 61mL of tert-butyl alcohol (Sigma-Aldrich, 99.7%) under continual stirring for 10 min. Concentrated HNO<sub>3</sub> was added until a pH of 3. The solution was heated to a temperature of 70°C and was maintained at that temperature for 10 min. It was later decreased to 60°C while a drop wise addition of 39 mL of zirconium n-butoxide was performed (Sigma-Aldrich, 80%).

Following the addition, the alkoxide mixture was maintained at a temperature of 70°C for 24 h under continual stirring and total reflux. This was followed by evaporation of the solvent and drying at 80°C in an oven for 24h.

For the case of Mn<sup>2+</sup> modified ZrO<sub>2</sub> catalysts (where M = Mn, Fe, Co, Ni and Cu), a quantity of nitrate corresponding to the ionized metal (Sigma-Aldrich, 99% purity) was dissolved in deionized water. The concentration of the resulting solution was 1% dispersed in the sol-gel zirconium oxide.

The obtained powders were calcined at 400°C for 12 h in air, with increasing rate of 2 °C/min from room temperature.

## 2.2. Samples characterization.

To determine the crystal phase and the crystallite size of our synthesized powders, X-ray diffraction (XRD) powder patterns were obtained using hand-pressed samples mounted on a Philips PW 1830 diffractometer using the Cu-K $\alpha$  line ( $\lambda=0.154$  nm). The crystal phases were identified by comparison with JCPDS cards and the crystallite size ( $D$ ) were calculated by X-ray line broadening analysis according to the Debye-Scherrer formula [16, 17].

$$D = \frac{0,9\lambda}{\beta \cos \theta} \dots\dots\dots(1)$$

Where  $\lambda$  (nm) is the X-ray wavelength and  $\beta$  (radians) is the full width at half-maximum (FWHM) of the diffraction peak.

In order to verify the presence of metals in the doped samples, these were analyzed by energy-dispersive spectroscopy (EDS), the analysis were carried out using a JOEL JSM-6610.

Absorption and reflectance spectra of prepared ZrO<sub>2</sub> were recorded by a Cary-1 (Varian) UV-Vis-NIR spectrophotometer equipped with an integrated sphere. BaSO<sub>4</sub> was used as a reference. The band gap of all materials can be estimated from the absorption edge wavelength of the inter band transition. The most accepted method for determining the band gap energy values of an insulator or semiconductor is by plotting the square root of the Kubelka-Munk function multiplied by the photon energy versus the photon energy and extrapolating the linear part of the rising curve to zero. For each material the optical band gap ( $E_g$ ) was calculated according the following equation [18]:

$$E_g(eV) = \frac{1239}{\lambda(\text{\AA})} \dots\dots\dots(2)$$

The typical N<sub>2</sub> adsorption isotherms for the ZrO<sub>2</sub> powders area are used to obtain detailed information about the pore size, the specific surface area, the meso-pore volume and the pore size distribution. A N<sub>2</sub> adsorption and desorption isotherm were performed on the ZrO<sub>2</sub> powders. The total surface area and pore volume were determined using the BET and the three point method, respectively.

## 2.3. Photocatalytic experiment.

The catalytic photodegradation studies were performed using the following procedure: 100 mg of photocatalyst were placed in 100mL of a solution of indigo carmine dye (20 mg/L) at their natural pH. The suspensions were kept in the dark for 30 min. The suspension was maintained under continual stirring in order to reach the adsorption equilibrium. Irradiation was carried out with external lamp (HPK 125 W UV lamp, Black light mercury HgV). Between the lamp and the glass reactor, a circulating water Pyrex-glass tank cooler was positioned. The suspension was homogenized by a magnetic stirrer and remained in contact with air [19]. During the photocatalytic test, 5mL of samples were taken at 20 min intervals over a period of 2h. Each sample was centrifuged at 1500 rpm using a Thermo-scientific SL-16 instrument for a period of 15 min and analyzed by T80-UV/Vis spectrophotometer ( $\lambda_{max}=611$  nm).

## 3. RESULTS SECTION

### 3.1. Structural properties.

Figure 1 shows the diffraction patterns of the samples treated at 400 °C. The presence of the tetragonal phase was observed to be dominant for zirconium oxide according to JCPDS card 42-1164 [20]. It was characterized by peaks located at  $2\theta$  value of 30, 35, 51 and 61°. Metal compounds were not observed due to the fact that the metal loadings are very small (1%). This zirconia phase has been reported to be the most active [21-26]. The synthesis method used enabled us to obtain this phase at a low temperature compared to the much higher temperature (1200°C) reported for this phase in the literature [22]. The average size of crystallites for the different photocatalysts is calculated from Scherrer's formula based on line broadening analysis and their values are tabulated in Table1. The sample Fe/ZrO<sub>2</sub> (9.75nm) has the lowest size while the higher is that of the sample Ni/ZrO<sub>2</sub> (14.35nm).

The Fe, Ni, Co, Mn and Cu incorporation and their percentage in doped ZrO<sub>2</sub> samples were analyzed by energy-dispersive X-ray (EDX) spectroscopy. The EDS spectra (Figure 2) show the characteristic peaks of Zr and O in all samples and they confirm the presence of doping elements in the doped samples

with low percentage (Table 1). In general, by EDX microanalysis, the major elements are quantitatively determined [27].

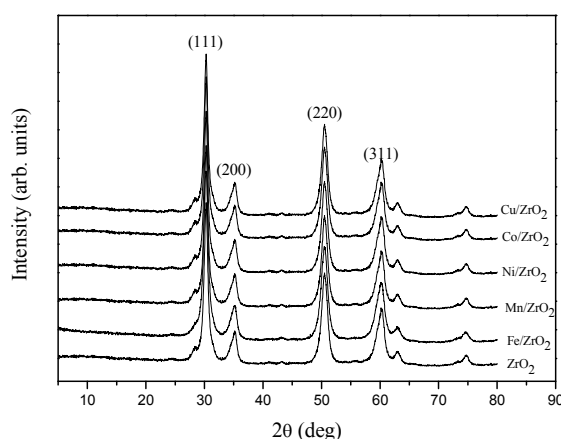


Figure 1. XRD patterns of undoped and doped ZrO<sub>2</sub> powders.

However, the accurate knowledge of the minor elemental composition down to trace concentration levels cannot be identified unambiguously by this technique because of the bremsstrahlung radiation that restricts the detection limit [28].

Figure 3 depicts the optical absorbance spectra for pure and doped ZrO<sub>2</sub> samples in the 200-600 nm wavelength regions. It can be seen that the maximum absorption for all materials is located in the UV light wavelength range. The energy values corresponding to the band gap levels (E<sub>g</sub>) were calculated for the catalysts treated at 400°C. Their behavior was studied and their results are shown in (Table 2). We observe that the doped samples of ZrO<sub>2</sub> with iron and copper show decreased values of E<sub>g</sub> in comparison to the reference (ZrO<sub>2</sub>, E<sub>g</sub>=4.0 eV). The lowest values were obtained for iron, the most active catalyst, at temperatures of 400°C. When zirconium oxide was doped with manganese, we observed a decrease in E<sub>g</sub>. In the spectra of the samples containing manganese, iron and cobalt treated at 400°C, bands in the visible region of the spectra were observed. This may be because the metal is located on the surface of the support and may have a different oxidation state. This is not observed for the materials containing Cu, Ni and the pure oxide. With respect to the value of E<sub>g</sub> there did not appear to be a trend with respect to the electronegativity of the dopant metal. This may be due to the fact that the dopant metals used were very similar. However, we should take note that the results obtained by XPS [6] show that the only metal not detected on the surface was nickel together with cobalt, these metals had the highest value for E<sub>g</sub> in the studied temperature. The objective, which we pursued by decreasing the value of E<sub>g</sub>, was to increase the photocatalytic activity [29, 30]. In addition, this would imply that in the future, radiation having a lower energy might be used in order to extend the response of the materials to include the visible region.

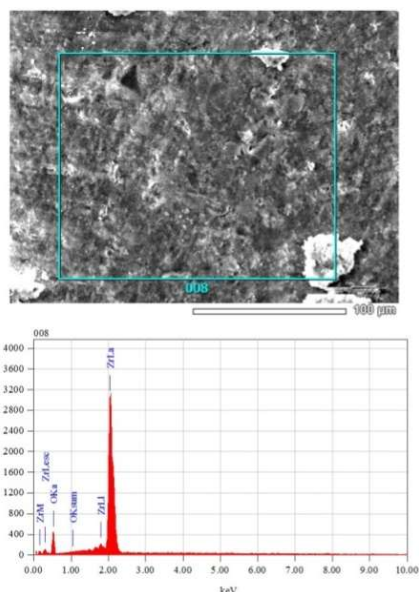


Figure 2. SEM and EDX analysis spectrum of undoped ZrO<sub>2</sub> powders.

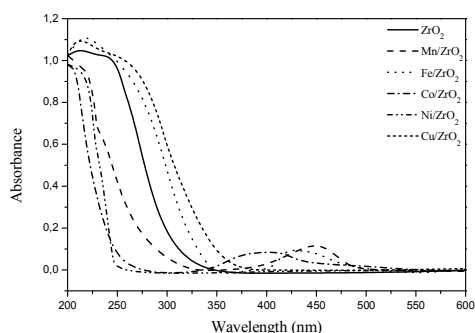


Figure 3. UV-Vis absorption spectra of pure and doped ZrO<sub>2</sub>.

N<sub>2</sub> adsorption-desorption isotherms pattern of undoped ZrO<sub>2</sub> and doped ZrO<sub>2</sub> samples with different transition metals are shown in Figure 4. All samples exhibit a typical type IV behavior, showing pore condensation with pronounced adsorption-desorption hysteresis loops. This indicates the existence of mesopores [31].

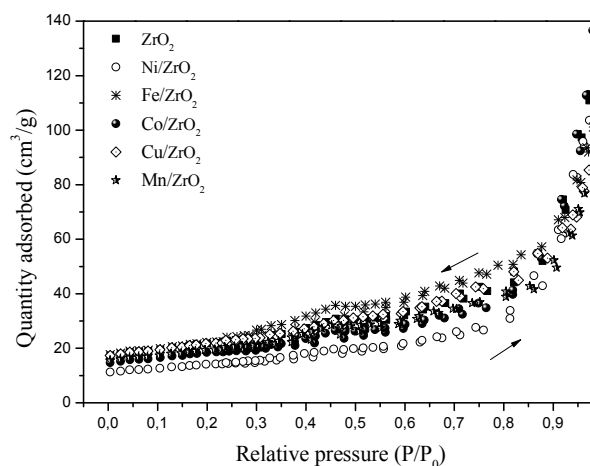


Figure 4. N<sub>2</sub> adsorption/desorption isotherms for undoped and doped ZrO<sub>2</sub>.

Specific surface area of the synthesized materials was determined using the Brunauer, Emmett, and Teller (BET) method. The specific surface area values are provided in Table 2. By comparison between the specific surface of the non-doped material and those of doped materials, we notice a decrease of the specific surface area due to the doping with the exception of iron that's the sample has a high specific surface.

### 3.2. Photocatalytic activity.

We have studied the photodegradation of indigo carmine over a period of 2h. The results of this study are shown in Figure 5 it was observed that degradation occurs only following the adsorption of radiation [23]. Over a 2 h-period only 45% of the compound could be removed. However, in the presence of Mn/ZrO<sub>2</sub>, 70% of the indigo carmine could be removed in half the time. The behavior of ZrO<sub>2</sub>, Co/ZrO<sub>2</sub> and Cu/ZrO<sub>2</sub> is very similar.

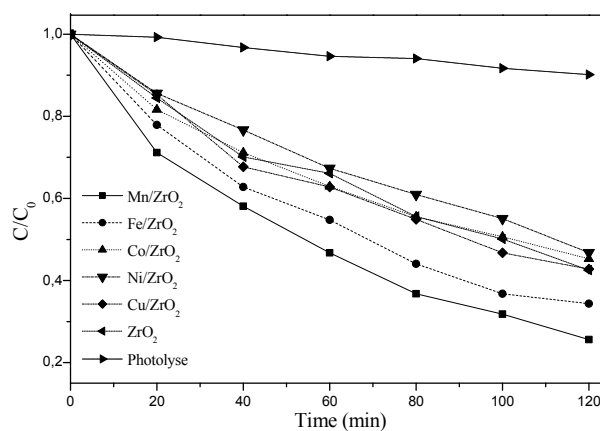


Figure 5. Degradation of Indigo Carmine as a function of time, where C<sub>0</sub> is the initial concentration (mg L<sup>-1</sup>) and C is the concentration at the time t.

Over a period of 1h they can degrade between 40 and 45% of the indigo carmine. The Fe/ZrO<sub>2</sub> catalyst shows an intermediate behavior, i.e degradation of 75% of the indigo carmine after 2h period. The results showed that Mn<sup>2+</sup>, and Fe<sup>2+</sup> ions can trap both

## Photocatalytic decolorization of indigo-carmine dye by sol-gel synthesized doped ZrO<sub>2</sub> photocatalyst

electrons and holes thus avoiding their recombination [32]: thus, doping ZrO<sub>2</sub> with these metal ions may contribute to a better activity than doping with Cu, Co, and Ni ions. The enhancement of the photocatalytic activity can be explained by the substitution of Zr<sup>4+</sup> by Mn<sup>3+</sup>, Fe<sup>2+</sup>, and/or Fe<sup>3+</sup> in the lattice. Also it would cause the formation of oxygen vacancies in the ZrO<sub>2</sub> lattice in order to maintain charge neutrality. Since the O<sup>2-</sup> anion is much larger than the cations, its removal upon vacancy formation would cause lattice contraction [33].

Photocatalytic degradation of organic contaminants usually follows pseudo-first order kinetics [24, 25]. By plotting  $\ln(C/C_0)$  as a function of time a straight line is obtained (Figure 6) being the slope of the different plots proportional to the rate constant of the photodegradation reaction. The apparent rate constant for photodegradation of the indigo carmine (Table 3) is  $0.718 \times 10^{-2} \text{ min}^{-1}$  for ZrO<sub>2</sub>, for Co/ZrO<sub>2</sub> and Ni/ZrO<sub>2</sub> it is  $0.702 \times 10^{-2}$  and  $0.626 \times 10^{-2}$ , this indicating that the modification of the zirconia phase with cobalt or nickel does not influence significantly the catalytic activity of the main phase. On the contrary on doping

with manganese or iron the catalytic activity of the ZrO<sub>2</sub> phase is greatly enhanced being the apparent rate constant equal to  $1.18 \times 10^{-2} \text{ min}^{-1}$  and  $0.978 \times 10^{-2} \text{ min}^{-1}$  respectively.

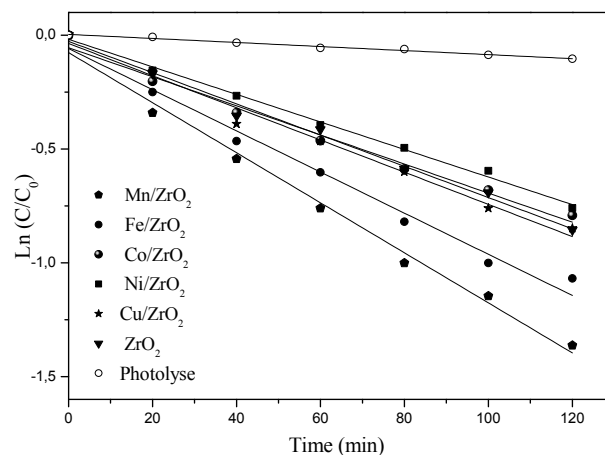


Figure 6. The plot of  $\ln(C/C_0)$  as a function of time.

Table 1. Compositional analysis of ZrO<sub>2</sub> of pure and doped ZrO<sub>2</sub> powders.

Samples	ZrO <sub>2</sub>	Mn/ ZrO <sub>2</sub>	Fe/ZrO <sub>2</sub>	Co/ZrO <sub>2</sub>	Ni/ ZrO <sub>2</sub>	Cu/ ZrO <sub>2</sub>
Oxygen (mass %)	24.26	25.07	26.13	24.59	25.52	24.88
Zirconium (mass %)	75.74	74.77	72.74	75.32	74.34	75.02
Dopant (mass %)	-	0.16	1.03	0.10	0.14	0.10

Table 2. The particle size,  $E_g$  and surface area of pure and doped ZrO<sub>2</sub>.

Photocatalyst	ZrO <sub>2</sub>	Mn/ ZrO <sub>2</sub>	Fe/ZrO <sub>2</sub>	Co/ZrO <sub>2</sub>	Ni/ ZrO <sub>2</sub>	Cu/ ZrO <sub>2</sub>
Crystallite size (nm)	9.86	11.66	9.75	12.72	14.35	10.11
$\lambda$ (nm)	307	276	335	227	249	334
$E_g$ (eV)	4.0	4.5	3.6	5.4	4.9	3.7
BET surface Area (m <sup>2</sup> /g)	92	78	96	65	57	83

Table 3. Kinetic parameters in photocatalytic degradation of Indigo Carmine.

Photocatalyst	ZrO <sub>2</sub>	Mn/ZrO <sub>2</sub>	Fe/ZrO <sub>2</sub>	Co/ZrO <sub>2</sub>	Ni/ZrO <sub>2</sub>	Cu/ZrO <sub>2</sub>	Photolysis
$k_1(\text{min}^{-1})$	0,00718	0,00718	0,00718	0,00718	0,00718	0,00718	0,00718
$k_2(\text{min}^{-1})$	0,00718	0,01188	0,00972	0,00702	0,00626	0,00749	8,47E-04
$k_2/k_1$	1	1,655	1,354	0,978	0,872	1,043	0,118
Standard Error	1,72E-04	3,43E-04	3,14E-04	2,44E-04	1,08E-04	2,26E-04	2,71E-05
Adj. R-Square	0,996	0,994	0,993	0,992	0,998	0,994	0,993

## 4. CONCLUSIONS

In this work, we confirm that Heterogeneous photocatalysis can be employed as a promising method for the decolorization of indigo carmine dye. All oxides synthesized and used as photocatalysts have a very large chemical stability and a high specific surface area which increases the amount of adsorbed dye. The energy values corresponding to the band gap levels ( $E_g$ ) were calculated for the catalysts treated at 400°C. We observe that the doped samples of ZrO<sub>2</sub> with iron and copper show decreased

values of  $E_g$  in comparison to the reference (ZrO<sub>2</sub>,  $E_g=4.0$  eV). The lowest values were obtained for iron, the most active catalyst, at temperatures of 400°C. Doping ZrO<sub>2</sub> with Mn and Fe showed high activity in the photodegradation of indigo carmine. We note that doping ZrO<sub>2</sub> with these metal ions may contribute to a better activity than doping with Cu, Co, and Ni ions. These results can be improved by increasing the doping level as well as the experimental conditions that can be considered in another study.

## 5. REFERENCES

- [1] Binitha N.N., Yaakob Z., Resmi R., Influence of synthesis methods on zirconium doped titania photocatalysts, *Central European Journal of Chemistry*, 8, 182-187, **2010**.
- [2] Gutiérrez-Segura E., Solache-Ríos M., Colín-Cruz A., Sorption of indigo carmine by a Fe-zeolitic tuff and carbonaceous material from pyrolyzed sewage sludge, *Journal of Hazardous Materials*, 170, 1227–1235, **2009**.
- [3] Lakshmi U.R., Srivastava V.C., Mall I.D., Lataye D.H., Rice husk ash as an effective adsorbent: Evaluation of adsorptive characteristics for Indigo Carmine dye, *Journal of Environmental Management*, 90, 710–720, **2009**.
- [4] Shikha Panchal, Ritu Vyas, Use of Undoped and Iron Doped Zirconium Dioxide in Photocatalytic Degradation of Malachite Green, *Scientific Reviews & Chemical Communications*, 3, 190-197, **2013**.
- [5] Kadi M. W., Mohamed R. M., Enhanced Photocatalytic Activity of ZrO<sub>2</sub>-SiO<sub>2</sub> Nanoparticles by Platinum Doping, *International Journal of Photoenergy*, **2013**.
- [6] López T., Alvarez M., Tzompantzi F., Picquart M., Photocatalytic degradation of 2,4-dichlorophenoxyacetic acid and 2,4,6-trichlorophenol with ZrO<sub>2</sub> and Mn/ZrO<sub>2</sub> sol-gel materials, *Journal of Sol-Gel Science and Technology*, 37, 207–211, **2006**.
- [7] Fox M. A., et Dulay M.T., Heterogeneous photocatalysis, *Chemical reviews*, 93, 341–357, **1993**.
- [8] Glaze W.H., Kang J.W., Advanced oxidation processes. Description of a kinetic model for the oxidation of hazardous materials in aqueous media with ozone and hydrogen peroxide in a semibatch reactor, *Industrial & engineering chemistry research*, 28, 1573–1580, **1989**.
- [9] Sreethawong T., Ngamsinlapasathian S., Yoshikawa S., Synthesis of crystalline mesoporous-assembled ZrO<sub>2</sub> nanoparticles via a facile surfactant-aided sol-gel process and their photocatalytic dye degradation activity, *Chemical engineering journal*, 228, 256–262, **2013**.
- [10] Botta S.G., J. Navío J.A., Hidalgo M.C., Restrepo G.M., Litter M.I., Photocatalytic properties of ZrO<sub>2</sub> and Fe/ZrO<sub>2</sub> semiconductors prepared by a sol-gel technique, *Journal of Photochemistry and Photobiology A: Chemistry*, 129, 89–99, **1999**.
- [11] Karunakaran C., Senthilvelan S., Photocatalysis with ZrO<sub>2</sub>: oxidation of aniline, *Journal of Molecular Catalysis A: Chemical*, 233, 1–8, **2005**.
- [12] Pouretedal H., Tofangrazi R. Z., Keshavarz M. H., Photocatalytic activity of mixture of ZrO<sub>2</sub>/SnO<sub>2</sub>, ZrO<sub>2</sub>/CeO<sub>2</sub> and SnO<sub>2</sub>/CeO<sub>2</sub> nanoparticles, *Journal of Alloys and Compounds*, 513, 359–364, **2012**.
- [13] Santos J.S. , Trivinho-Strixino F., Pereira E.C., The influence of experimental conditions on the morphology and phase composition of Nb-doped ZrO<sub>2</sub> films prepared by spark anodization, *Corrosion Science*, 73, 99–105, **2013**.
- [14] Urlacher C., Dumas J., Serughetti J., Mugnier J., Munoz M., Planar ZrO<sub>2</sub> waveguides prepared by the sol-gel process: Structural and optical properties, *Journal of Sol-Gel Science and Technology*, 8, 999–1005, **1997**.
- [15] Urlacher C., De Lucas C. M., Bernstein E., Jacquier B., Mugnier J., Study of erbium doped ZrO<sub>2</sub> waveguides elaborated by a sol-gel process, *Optical Materials*, 12, 19–25, **1999**.
- [16] Alex H.C., Chan John F., Porter J.P., Barford, C., Chan.K. , Effect of Thermal Treatment on the Photocatalytic Activity of TiO<sub>2</sub> Coatings for Photocatalytic Oxidation of Benzoic Acid, *Journal of Materials Research*, 17, 1758-1765, **2011**.
- [17] Carpio E., Zuniga P., Ponce S, Solis J, Rodriguez J., Estrada W., Photocatalytic degradation of phenol using TiO<sub>2</sub> nanocrystals supported on activated carbon, *Journal of Molecular Catalysis A: Chemical*, 228, 293–298, **2005**.
- [18] Azhagan S.A.C., Ganesan S., Effect of zinc acetate addition on crystal growth, structural, optical, thermal properties of glycine single crystals, *Arabian Journal of Chemistry*, **2013**.
- [19] Benhebal H., Chaib M., Léonard A., Stéphanie D., Crine M., Synthesis, characterization and photocatalytic properties of alkali metals doped tin dioxide, *Journal of Molecular Structure*, 1004, 222-226, **2011**.
- [20] Yang X., Jentoft R.E., Jentoft F.C., n-Butane isomerization catalyzed by sulfated zirconia nanocrystals supported on silica or  $\gamma$ -alumina, *Catalysis letters*, 106, 195–203, **2006**.
- [21] Srinivasan R., Watkins T., Hubbard C., Davis B.H., Sulfated zirconia catalysts. The crystal phases and their transformations, *Chemistry of materials*, 7, 725–730, **1995**.
- [22] Wells A.F, Structural inorganic chemistry, *Oxford University Press*, **2012**.
- [23] Murcia J.J., Hidalgo M.C., Navío J.A., Araña J., Doña-Rodríguez J.M., Correlation study between photo-degradation and surface adsorption properties of phenol and methyl orange on TiO<sub>2</sub> Vs platinum-supported TiO<sub>2</sub>, *Applied Catalysis B: Environmental*, 150, 107–115, **2014**.
- [24] Neppolian B., Sakthivel S., Arabindoo B., Palanichamy M., Murugesan V., Kinetics of photocatalytic degradation of reactive yellow 17 dye in aqueous solution using UV irradiation, *Journal of Environmental Science and Health, Part A*, 36, 203–213, **2001**.
- [25] Turchi C.S., Ollis D.F., Photocatalytic degradation of organic water contaminants: mechanisms involving hydroxyl radical attack, *Journal of catalysis*, 122, 178–192, **1990**.
- [26] Kokporika L., Onsuratoom S., Puangpetch T, Chavadej S., Sol-gel-synthesized mesoporous-assembled TiO<sub>2</sub>-ZrO<sub>2</sub> mixed oxide nanocrystals and their photocatalytic sensitized H<sub>2</sub> production activity under visible light irradiation, *Materials Science in Semiconductor Processing*, 16, 667–678, **2013**.
- [27] Van Grieken R., Markowicz A., *Handbook of X-ray Spectrometry*, CRC Press, **2001**.
- [28] Martínez-Criado G., Optical investigation of ZnO nanowires, *Acta Physica Polonica A*, 117, 369–373, **2010**.
- [29] Ba-Abbad M.M., Kadhum A.A.H., Mohamad A.B., Takriff M.S., Sopian K., Visible light photocatalytic activity of Fe<sup>3+</sup>-doped ZnO nanoparticle prepared via sol-gel technique, *Chemosphere*, 91, 1604–1611, **2013**.
- [30] Kazemi M., Mohammadzadeh M.R., Superhydrophilicity and photocatalytic activity of sol-gel deposited nanosized titania thin films, *Thin Solid Films*, 519, 6432–6437, **2011**.
- [31] Lu R., Tangbo H., Wang Q., Xiang S., Properties and characterization of modified HZSM-5 zeolites, *Journal of Natural Gas Chemistry*, 12, 56–62, **2003**.
- [32] Dholam R., Patel N., Adami M, Miotello A., Hydrogen production by photocatalytic water-splitting using Cr-or Fe-doped TiO<sub>2</sub> composite thin films photocatalyst, *International Journal of Hydrogen Energy*, 34, 5337–5346, **2009**.
- [33] Lin M.Z, Chen H., Chen W.F., Nakaruk A., Koshy P., Sorrell C.C., Effect of single-cation doping and codoping with Mn and Fe on the photocatalytic performance of TiO<sub>2</sub> thin films, *International journal of hydrogen energy*, 39, 21500–21511, **2014**.

## 6. ACKNOWLEDGEMENTS

Belkacem Ziane would like to thank the staff of the laboratory of chemistry, faculty of sciences of matter IBN Khaldoun University of Tiaret for synthesis and characterization, and thanks Prof El-habib Belarbi (laboratory synthesis and catalysis) for her help.

© 2017 by the authors. This article is an open access article distributed under the terms and conditions of the Creative Commons Attribution license (<http://creativecommons.org/licenses/by/4.0/>).

7. SUPPLEMENTARY FILES

